Desalination and Water Treatment
www.deswater.com
doi: 10.5004/dwt.2023.29324

286 (2023) 173–182
February

Enhanced fluoride removal using alumino urea gel synthesized by a facile hydrothermal method

Mingshan Song, Shushu Li, Changqing Ye*

Department of Health Inspection and Quarantine, School of Public Health, Nantong University, 9 Seyuan Road, Jiangsu 226019, China, Phone No.: +86-136-1523-5761; email: cqye@ntu.edu.cn (C. Ye), Phone No.: +86-198-2703-3885; email: 2216718680@qq.com (M. Song), Phone No.: +86-188-5521-5921; email: 3045524693@qq.com (S. Li)

Received 19 September 2022; Accepted 21 January 2023

ABSTRACT

Fluoride with high amounts in drinking water is harmful to human's health. In this study, an aluminum-urea gel adsorbent (AUG) was synthesized using aluminum chloride and urea as raw materials based on a simple one-pot hydrothermal method and applied for the defluoridation of drinking water. The structures of AUG were characterized and its defluoridation performance was evaluated. Our experimental results showed that the surface of AUG was amorphous with rich functional groups and its efficiency for fluoride removal exceeded 90% in the pH range of 5.0–8.0 with good stability. The fluoride adsorption isotherm of AUG could be fitted well with Langmuir with its maximum adsorption capacity at 107.7 mg/g. The pseudo-second-order model implied that the adsorption mechanism of fluoride on AUG was mainly based on chemical reactions between fluoride and the ligands between unsaturated aluminium and carbon functional groups. In addition, ion exchange effect and electrostatic attraction may also help the adsorption. Our study suggests that AUG might become a potential defluoridation agent for drinking water.

Keywords: Aluminum; Urea; Adsorption; Fluoride removal; Hydrothermal synthesis

1. Introduction

Fluorine is one of the necessary trace element with certain physiological functions mostly found in human teeth and bones [1]. A moderate intake of fluoride can help prevent dental caries in children and brittle bones in the elderly, but excessive intake will cause dental fluorosis, bone fluorosis [2,3]. Fluorosis can cause damage to the immune system and kidneys, and even endanger life [4,5]. Both natural environmental factors and production activities can cause pollution of fluoride in water bodies [6,7]. For example, such pollution exists in most parts of China [8], especially in remote rural areas in northern China [9]. In this regard, the World Health Organization has set a limit of 1.5 mg/L for the concentration of fluoride in drinking water [10], and China Sanitation Standards for Drinking Water (GB 5749-2006) stipulates that the upper limit of fluoride quality concentration in drinking water is 1.0 mg/L [11].

At present, main methods of removing fluoride from water include electric flocculation [12], coagulation and precipitation, ion exchange [13], reverse osmosis and adsorption [14], among which adsorption is considered to be one of the most ideal ways because of its simple operation and low cost [15]. Traditionally, activated alumina [3] and other low-cost aluminum-based adsorbents have been widely used for fluoride removal [16]. However, the alumina adsorbent has some disadvantages such as low adsorption capacity, acidic application range, poor adsorption kinetics and regeneration difficulties [17,18]. Many efforts have been put on modification of aluminum-based and alternative adsorbents to enhance the efficiency of fluoride removal with various materials, such as MOF [19], carbon [20] and

* Corresponding author.

graphene-based composites [6], LDH [21], rare earth doped materials [22] and biomass materials [23] etc, Sathish et al. [24] increased the fluoride removal ability by 3–5 times by coating zirconium metal on the surface of carbon material. Dhanasekaran and Sahu [16] chemically modified sawdust with ferric hydroxide and activated alumina as adsorbents to remove arsenic and fluoride from groundwater with an adsorption capacity of 2.42 mg/g.

Recently, it has been found that some special structures of aluminum oxide, such as defects, could significantly improve the ability of fluoride removal, which has aroused interests in the study of fluoride removal using aluminum oxide. It needs to be emphasized that there are many intermediate transition states for aluminum oxide except three stable crystal phases since the hydrolysis process of aluminum salt is complex. In particular, the amorphous form of aluminum oxide is considered to be favorable for fluoride removal. For examples, Gong et al. [25] have investigated the defluoridation performance of different alumina structures, suggesting that low-temperature calcined alumina precipitation has high defluorination efficiency. Kang et al. [26] implied that high-temperature treatment of aluminum oxide could be conducive for the formation of defects and promote the adsorption of fluoride. Such investigations revealed that aluminum oxides with different structures could be obtained with different preparation methods, which would significantly impact on the adsorption of fluoride.

In this study, an aluminum-urea gel adsorbent (AUG) for defluoridation was successfully prepared based on slowly hydrothermal hydrolysis of aluminum solution containing urea. The as-prepared adsorbent has the advantages of convenient operation, low-cost and high efficiency on adsorption of fluoride. We evaluated the AUG adsorbent in terms of: the structural characterization, the adsorption capacity for fluoride, model fitting, and possible defluoridation mechanisms.

2. Materials and research methods

2.1. Reagents and chemicals

Chemical reagents (NaF, $AlCl_3$, HNO_3, NaOH, and CH_4N_2O) were used in this study. The reagents used were all of analytical grade, and were used without further purification. 1 g/L fluoride stock solution was prepared with NaF and deionized water. Adsorption working solution of various concentrations was diluted from the stock solution with deionized water.

2.2. Materials synthesis

At room temperature, a quantity of $AlCl_3$ and CH_4N_2O, with volume ratio of 1: 1.1; molar ratio of 1:2, was mixed together and the mixture was transferred into a hydrothermal autoclave with a capacity of 50 mL and heated at 100°C for 12 h. After the reaction had cooled down, the contents were washed and centrifuged 2–3 times to remove the unreacted reactant from the surface. The washed samples were dried to constant weight at 90°C in a blast drying oven, and then ground in a mortar, and recorded as AUG for later use.

2.3. Materials characterization

The morphology of the samples was analyzed by scanning electron microscopy (SEM) (Gemini SEM 300, Germany). Before the analysis, the samples were coated with gold sputtering to reduce the charging effect in the microscope. The specific surface area was determined by nitrogen chemisorption measurement and a specific surface area analyzer (Mac ASAP2460). The composition and crystal structure of the sorbents were analyzed by X-ray powder diffractometer (XRD) (Ultima IV, Japan). Fourier-transform infrared spectroscopy (FTIR) (TENSOR 27, Germany) was used to study the changes of functional groups on the AUG. X-ray photoelectron spectroscopy (XPS) (K-Alpha$^+$, America) was used to analyze the changes of surface elements on the AUG. The precipitation of aluminum was measured by an inductively coupled plasma optical emission spectrometer (ICP) (NexION 350). The zeta potential of the samples was measured by a nano-Zetasizer ZS90 instrument.

2.4. Adsorption experiments

Batch adsorption experiments were carried out in polyethylene tubes containing aqueous fluoride solution, varying the contact time (10 min to 24 h), pH range (3.0–11.0), initial fluoride concentration (4–90 mg/L) and adsorbent dose (0.15–0.3 g/L). These tubes were stirred at 140 rpm for a predetermined contact time using a constant temperature (at 25°C ± 1°C) shaker. The pH was adjusted by addition of NaOH (0.1 M) or HNO_3 (0.1 M) solution. When adsorption was finished, the sample was passed through a 0.45 μm membrane and was filtered by a vacuum suction pump, and the fluoride concentration of filtrate was measured by a fluoride ion-selective electrode.

2.5. Determination of adsorption capacity

The adsorption capacity of fluorine, q_e (mg/g), was calculated by Eq. (1) [27]:

$$q_e = \frac{\left(C_0 - C_e\right)V}{m} \tag{1}$$

where C_0 (mg/L) is the initial fluorine concentration; C_e (mg/L) is the fluorine concentration at equilibrium; V (L) is the volume of fluoride solution and m (g) is the mass of adsorbent.

3. Results and discussion

3.1. Characterization of materials

Fig. 1a illustrates that the SEM images of AUG exhibited a solid surface without obvious pore structure. Fig. 1b shows that after adsorption of fluoride the surface of AUG was somewhat crunched with many more particles appearing. Such adsorption could be further confirmed by energy-dispersive X-ray spectroscopy (EDS) images (Fig. 1c and d). Fig. 2a exhibits the N_2 adsorption–desorption isotherms and pore size distribution of AUG. The XRD image (Fig. 2b) shows that after absorbing fluoride, the surface of AUG was still amorphous with no obvious change.

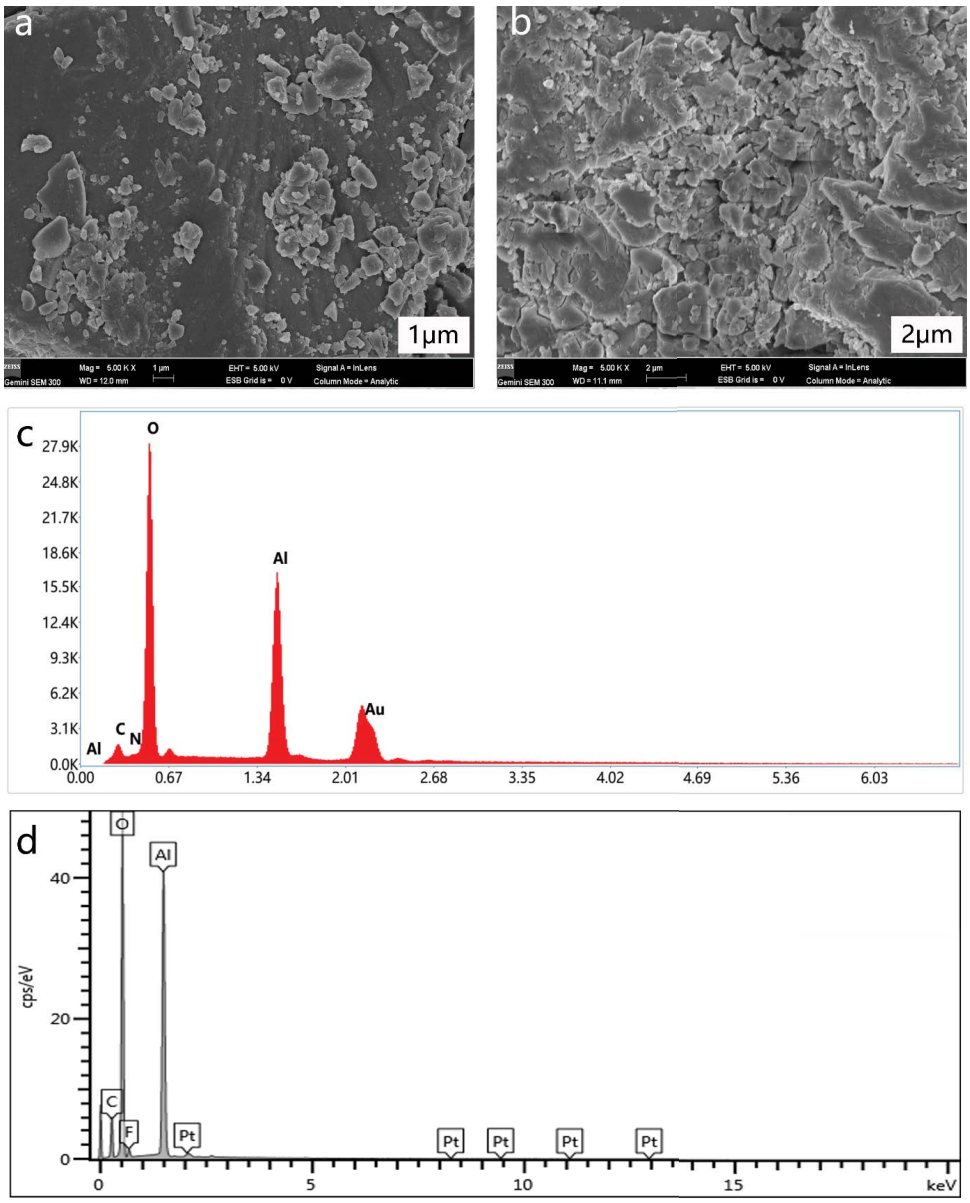

Fig. 1. (a) SEM of AUG, (b) SEM of AUG after fluoride adsorption, (c) EDS of AUG, and (d) EDS of AUG after fluoride adsorption.

The N_2 adsorption–desorption isotherm of the AUG was mainly an H_3-type hysteresis loop, which is characteristic for mesoporous structure. The distribution diagram of pore sizes also confirms the existence of mesoporous (2–50 nm) structure. The results of the BET analysis suggested that the BET surface areas of AUG were 1.5621 m^2/g and its pore volumes were 0.006735 cm^3/g. Such results implied that physical adsorption might not be the main process for adsorption of fluoride on AUG. Based on the XRD pattern of AUG (Fig. 2b), no obvious crystallization peaks could be observed. Such results revealed that the prepared AUG was mainly in the form of an amorphous alumina phase.

Fig. 3 shows the chemical composition of AUG analyzed by XPS, indicating signals of Al 2p, C 1s, and O 1s. The high resolution XPS spectra of C 1s (Fig. 3b) can be fitted into three main peaks at 284.8, 285.84 and 289.39 eV, belonging to C–C, C–O, and C=O, respectively [26,28]. As shown in Fig. 3c, the two peaks in the O 1s spectrum at 532.08 and 532.73 eV, which can be assigned to C–O and adsorbed water (H_2O) on the AUG, respectively [29]. The peak at 531.28 eV belongs to Al–O in the adsorbent [26]. The peak at 74.68 eV in the Al 2p spectrum (Fig. 3d) is corresponding to alumina in AUG [30].

Fig. 4 shows FTIR spectra of the AUG before and after the adsorption of fluoride. The board peak at 3,361–3,042 cm^{-1} could be attributed to the stretching vibration of hydroxyl groups (–OH) associated with the carboxylic groups. The peak at 1,632 cm^{-1} corresponded to the stretching vibration of C=C [31]. The strong peak at 1,402 cm^{-1} could be assigned to the asymmetric stretching vibration mode of C=O [26].

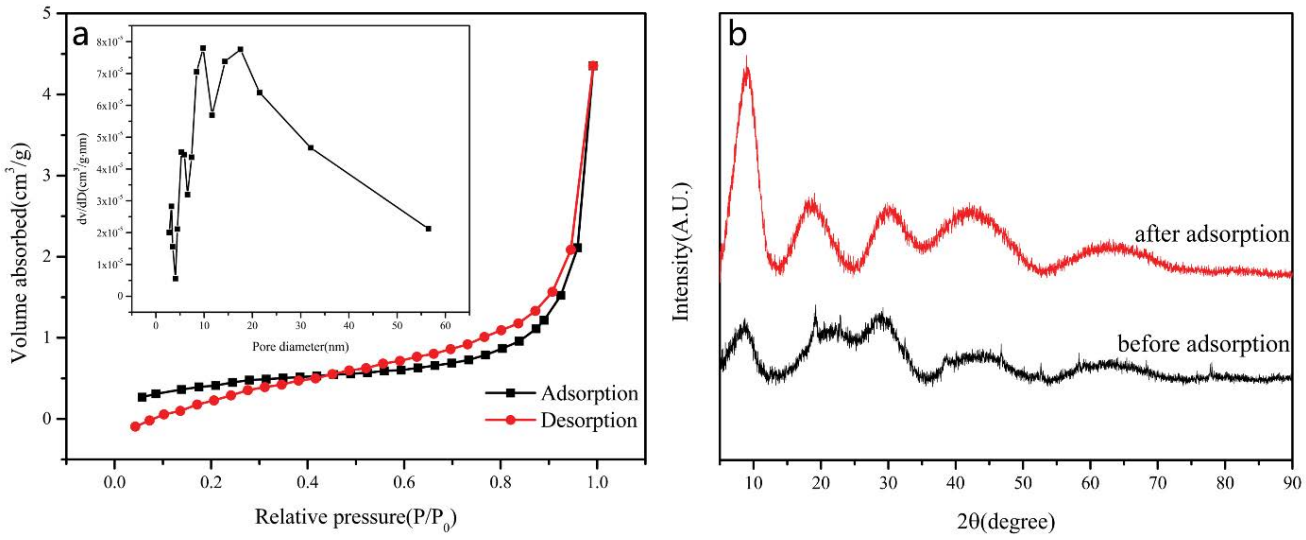

Fig. 2. (a) N_2 adsorption–desorption isotherms and (inset) the corresponding pore size distribution curve and (b) XRD patterns of the AUG.

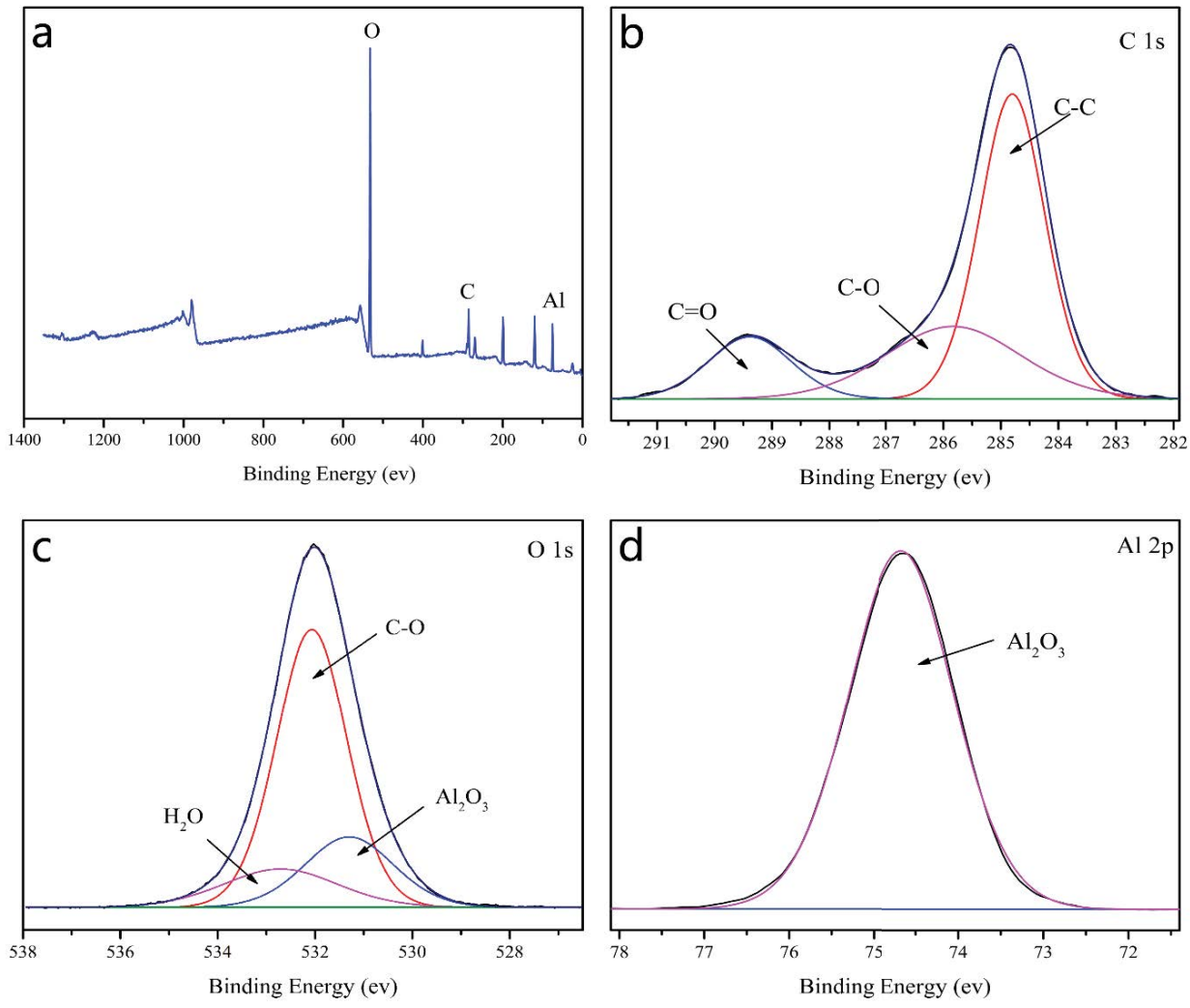

Fig. 3. XPS spectra of the AUG: (a) full range spectrum and high-resolution of (b) C 1s, (c) O 1s and (d) Al 2p.

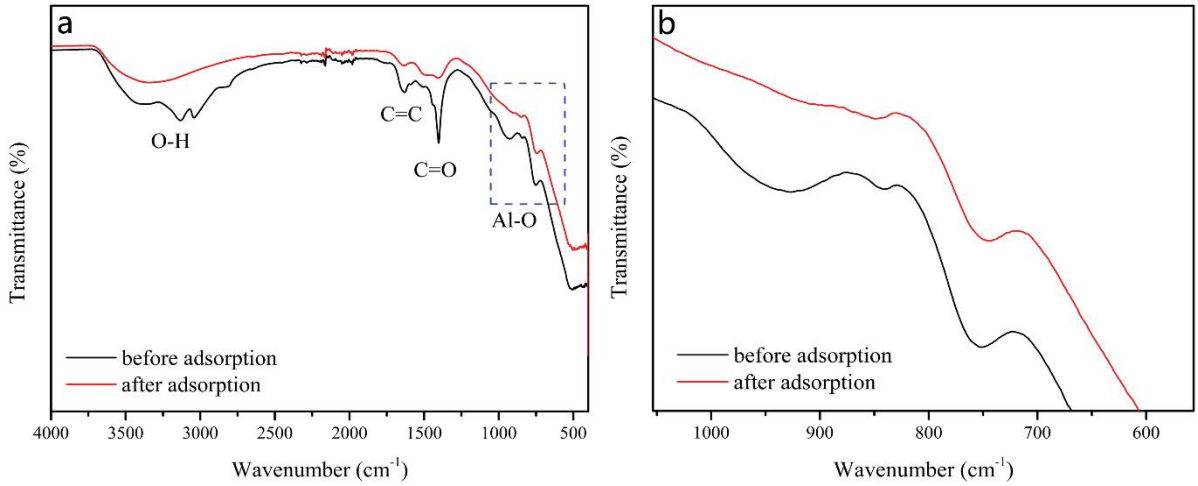

Fig. 4. FTIR spectra of the AUG before and after adsorption fluoride, (a) 1,400–400 cm^{-1} range and (b) 1,050–600 cm^{-1} range.

The peak at 927 cm^{-1} could be ascribed to vibrational of Al–O [32]. The peak at 751 cm^{-1} was attributed to the vibration of Al–O in AlO_6 octahedron [33].

3.2. Adsorption performance

3.2.1. Effect of AUG dose

Fig. 5 shows the effect of the AUG dose on fluoride removal when the pH value is 7.0 ± 0.1. With the increase of the dose from 0.15 to 0.3 g/L, generally the efficiency of fluoride removal increased from 88% to 98% while the capacity of fluoride adsorption decreased from 21.9 to 12.2 mg/g. Such results suggested that the increase of AUG would lead to the increase of of adsorption sites. Moreover, it could be found that the efficiency of fluoride removal enhanced significantly as the adsorbent dose increased from 0.15 to 0.25 g/L. With the further increase of the dose, the efficiency increased slowly. Considering the cost and the efficiency, the AUG dose of 0.25 g/L was selected for following experiments.

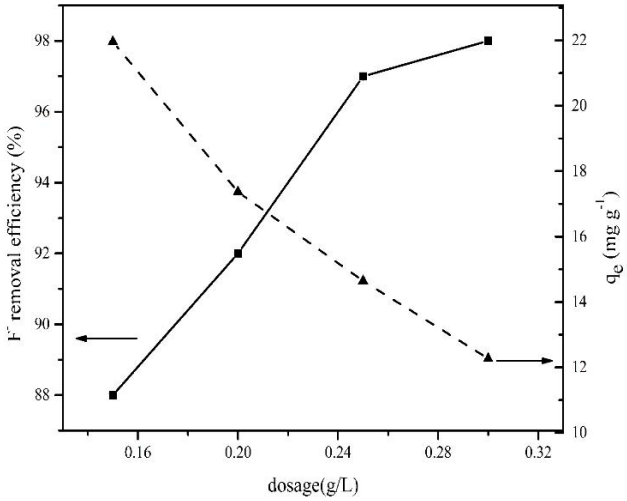

Fig. 5. The fluoride removal efficiency with elevated dosages of the AUG at pH 7.0. [Experimental conditions: C_0 = 4 mg/L, volume = 40 mL, and time = 20 h].

3.2.2. Effect of pH

Fig. 6 illustrates that the efficiency of fluoride removal increased gradually with the increase of the pH value of the solution from 3.0 to 8.0. The efficiency decreased rapidly with further increase of the pH value. Such results revealed that the AUG adsorbent was effective in removing fluoride when the pH value was in a certain range.

In aqueous solution, the zero-point charge (ZPC) of the adsorbent could affect the adsorption process of the adsorbent. Fig. 6 exhibits that the pH_{ZPC} value of the AUG was around 9.7. When pH < pH_{ZPC}, the adsorbent surface was positively charged, which is beneficial for enhancement of the electrostatic attraction and ligand/anion-exchange reaction between fluoride anions and adsorbent surface, leading to improvement of the adsorption capacity. When pH was in the range of 3.0–8.0, the zeta potential value remained above 29 mV, suggesting that protons in acidic suspension had little effect on the zeta potential of AUG.

When pH > pH_{ZPC}, deprotonation could cause the adsorbent surface to be negatively charged so that the electrostatic force would repel the adsorption of fluoride [34]. Meanwhile, the OH^- and fluoride anions in the solution would compete for adsorption on the adsorbent, resulting in decrease of fluoride adsorption [35]. However, when the pH value was in the range of 8.0 to 9.0 (lower than pH_{ZPC}) and the adsorbent was positively charged, the adsorption capacity of fluoride decreased rapidly, implying that defluoridation was not only influenced by electrostatic interaction. Because the maximum efficiency of fluoride removal could be obtained at the pH value of 7.0, which is close to the drinking water, this pH was adopted for evaluation of the performance of the adsorbent.

3.2.3. Adsorption isotherm

Fig. 7 illustrates the impact of initial fluorine concentration on the efficiency of fluoride removal. It could be observed

that with the increase of fluoride concentration from 4 to 90 mg/L, the fluoride adsorption capacity of AUG significantly increased in the beginning and then almost reached a plateau. Such results suggested that fluoride with increased concentration could gradually occupy all the active sites of the adsorbent. The adsorption capacity of AUG reached 83.81 mg/g for saturation.

Freundlich and Langmuir models were applied for analysis of the adsorption behavior of fluoride on adsorbents [36]. Theoretically, Langmuir isotherm equation was considered as the monolayer adsorption of the active site of the adsorbent while Freundlich isotherm equation was based on multi-layer adsorption on heterogeneous surfaces [37].

Freundlich isotherm could be presented with the following equation:

$$\log q_e = \log K_F + \frac{1}{n}\log C_e \tag{2}$$

where q_e (mg/g) is the equilibrium uptake of fluorine per unit mass of adsorbent, C_e (mg/L) is the equilibrium concentration of fluorine, K_F is the adsorption capacity, and $1/n$ is the adsorption strength.

Langmuir isotherm could be presented with:

$$\frac{C_e}{q_e} = \frac{1}{q_m K_L} + \frac{C_e}{q_m} \tag{3}$$

where q_e (mg/g) is the equilibrium uptake of fluorine per unit mass of adsorbent, q_m (mg/g) is the maximum adsorption, K_L (L/mg) is the Langmuir equilibrium constant, C_e (mg/L) is the equilibrium concentration of fluorine.

Fig. 7 shows the fitting curves and Table 1 lists the calculated parameters accordingly. It needs to be emphasized that the linear correlation coefficient (R^2) was normally used to evaluate the fitting model. It could be found that Langmuir model was more suitable to describe the adsorption process of fluoride on AUG, implying that the adsorption might be monolayer. From the Langmuir model the maximum adsorption capacity was calculated to be 107.7 mg/g, which is higher than that of adsorbents in previous reports (Table 2).

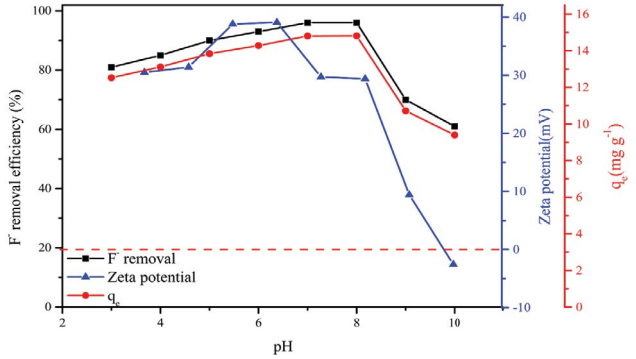

Fig. 6. Effect of pH on fluoride adsorption capacity and zeta potential of the AUG. [Experimental conditions: C_0 = 4 mg/L, adsorbent dose of 0.25 g/L, and time = 20 h].

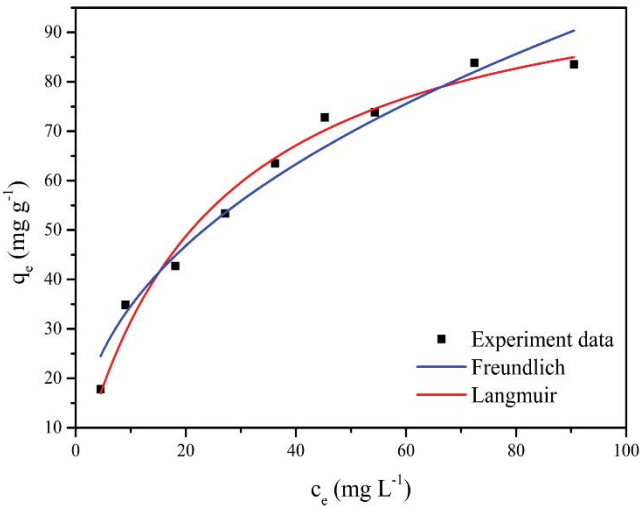

Fig. 7. Fitting curves of fluoride adsorption by Langmuir and Freundlich models. [Experimental conditions: C_0 = 4–90 mg/L, adsorbent dose of 0.25 g/L, pH = 7.0 ± 0.1, and time = 20 h].

3.2.4. Adsorption kinetics

Fig. 8 illustrates the kinetics of fluoride adsorption on AUG. It could be observed that the adsorption increased rapidly at the initial stage (t < 60 min) and then slowly. Such results might be attributed to the low concentration of residual fluoride and depletion of the active site after 60 min of the reaction [42]. The removal of fluorine by the AUG could reach 92% in the first 60 min, implying that the adsorption was fast and effective. The Lagergren kinetic model was then used to describe the kinetic behavior of the adsorbent and

Table 1
Adsorption isotherms parameters for fluoride adsorption [experimental conditions: C_0 = 4–90 mg/L, adsorbent dose of 0.25 g/L, pH = 7.0 ± 0.1, and time = 20 h]

Freundlich parameters			Langmuir parameters		
K_F (mg/g)	n	R^2	q_m (mg/g)	K_L (L/mg)	R^2
12.70	2.30	0.96	107.70	0.04	0.98

Table 2
Maximum adsorption capacities of different absorbents for fluoride

Adsorbents	q_{max} (mg/g)	C_0 (mg/L)	pH	References
Fe_3O_4@mSiO$_2$@mLDH	28.5	0–30	7.5	[38]
Y-Zr-Al tri-metal	31.0	10–300	7.0	[22]
Zr-Al-La	90.5	20–140	3.0	[39]
Acid modified alumina	69.5	27–968	6.5	[36]
Sulfate-doped Fe_3O_4/Al_2O_3 nanoparticles	70.4	2–160	7.0	[40]
Montmorillonite clay	40	0–50	5.0	[41]
AUG	107.7	4–90	7.0	This work

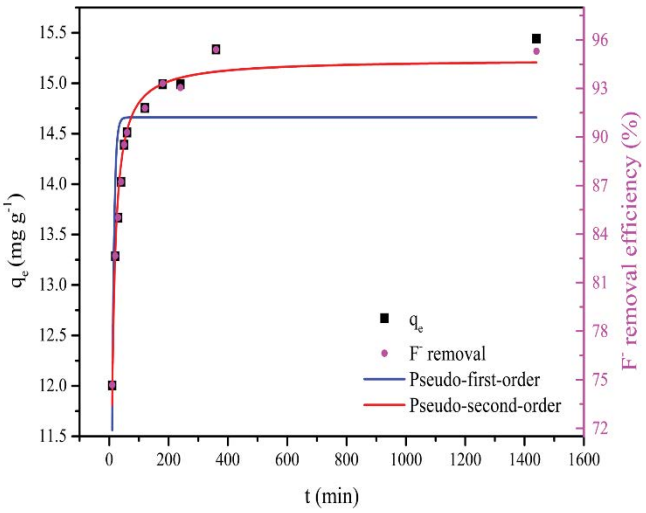

Fig. 8. Fitting curves of fluoride adsorption by pseudo-first-order kinetic plots and pseudo-second-order kinetic plots. [Experimental conditions: C_0 = 4 mg/L, adsorbent dose of 0.25 g/L, and pH = 7.0 ± 0.1].

evaluate the kinetic mechanism of the fluorine adsorption process.

The pseudo-first-order model:

$$\ln\left(q_e - q_t\right) = \ln q_e - k_1 t \tag{4}$$

The pseudo-second-order model:

$$\frac{t}{q_t} = \frac{1}{k_2 q_e^2} + \frac{t}{q_e} \tag{5}$$

where q_e and q_t are the adsorption capacities (mg/g) at equilibrium and at any point in time, respectively; k_1 and k_2 are the rate constants for the two models, respectively; t is the reaction time (min).

Fig. 8 shows the kinetics parameters calculated from the fitting plots and Table 3 lists the model parameters extracted from the fitting curve. It could be found that the pseudo-second-order model has the highest R^2 (>0.97) value and is more suitable for describing the kinetic behavior of adsorption on this adsorbent, implying that the rate-limiting step of fluorine adsorption on AUG was chemical adsorption.

3.2.5. Stability of AUG

Fig. 9 exhibits the influence of the pH value on the stability of AUG. It could be observed that large amounts of aluminum ions could be dissolved from AUG when the pH value is less than 7.0 and higher than 10.0. When the pH value was ranging from 7.0 to 10.0, the amounts of dissolved aluminum ions is below 0.2 mg/L [33]. When aluminum was dissolved from AUG, soluble aluminum and fluoride would form Al–F, which could not remove the fluoride in the solution, resulting in the deterioration of defluoridation efficiency. It is noteworthy that strongly acidic and basic conditions rarely occur. However, the stability of AUG in pH 7–10 was satisfactory enough for the removal of fluoride from drinking water.

Table 3
Kinetic models parameters for fluoride adsorption [experimental conditions: C_0 = 4 mg/L, adsorbent dose of 0.25 g/L, and pH = 7.0 ± 0.1]

Pseudo-first-order parameters			Pseudo-second-order parameters		
q_e (mg/g)	k_1 (g/mg·min)	R^2	q_e (mg/g)	k_2 (g/mg·min)	R^2
14.66	0.16	0.66	15.24	0.02	0.97

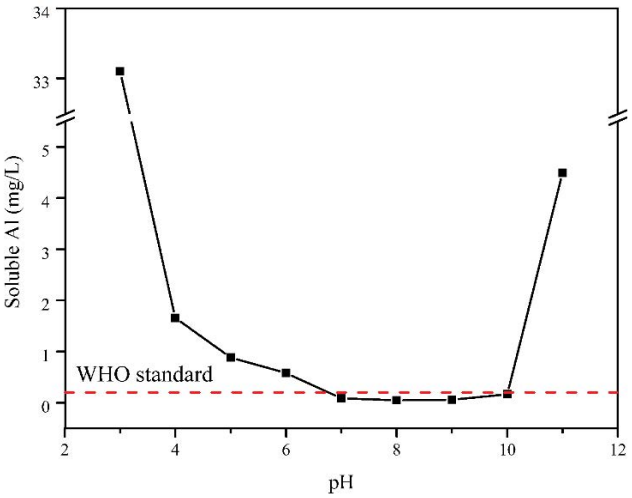

Fig. 9. Soluble Al concentration in AUG.

3.3. Adsorption mechanism

Fig. 10 illustrates the XPS results of the AUG after adsorption of fluoride. Compared with Fig. 3a, a new peak appeared at 686.05 eV (Fig. 10a), which belongs to the F 1s signal of fluorine. The high-resolution XPS of F 1s could be splitted into two peaks located at 685.15 and 689.33 eV. Because the binding energy of NaF is 684.5 eV [43,44], F does not exist in the form of NaF on the adsorbent surface. The peak at 685.15 eV can be attributed to Al–F in $NaAlF_6$, meaning that F forms an aluminum fluoride compound with Al in AUG [45]. The peak at 689.33 eV belongs to C–F [46], implying that the C element in the urea not only exists in the formation of the AUG material but also combined with F ions in the fluoride removal process, which could enhance the removal rate of fluoride. The intensity differences of C=O in Figs. 3b and 10b suggested that this peak is significantly reduced after the adsorption of fluoride, which further supports the combination of C with fluoride. As shown in Fig. 10c, the disappearance of H_2O suggested the involvement of the hydroxyl group in the fluoride removal process. Fig. 10d shows that the peak of Al 2p moved from 74.68 to 74.48 eV, indicating participation of Al in the defluoridation process.

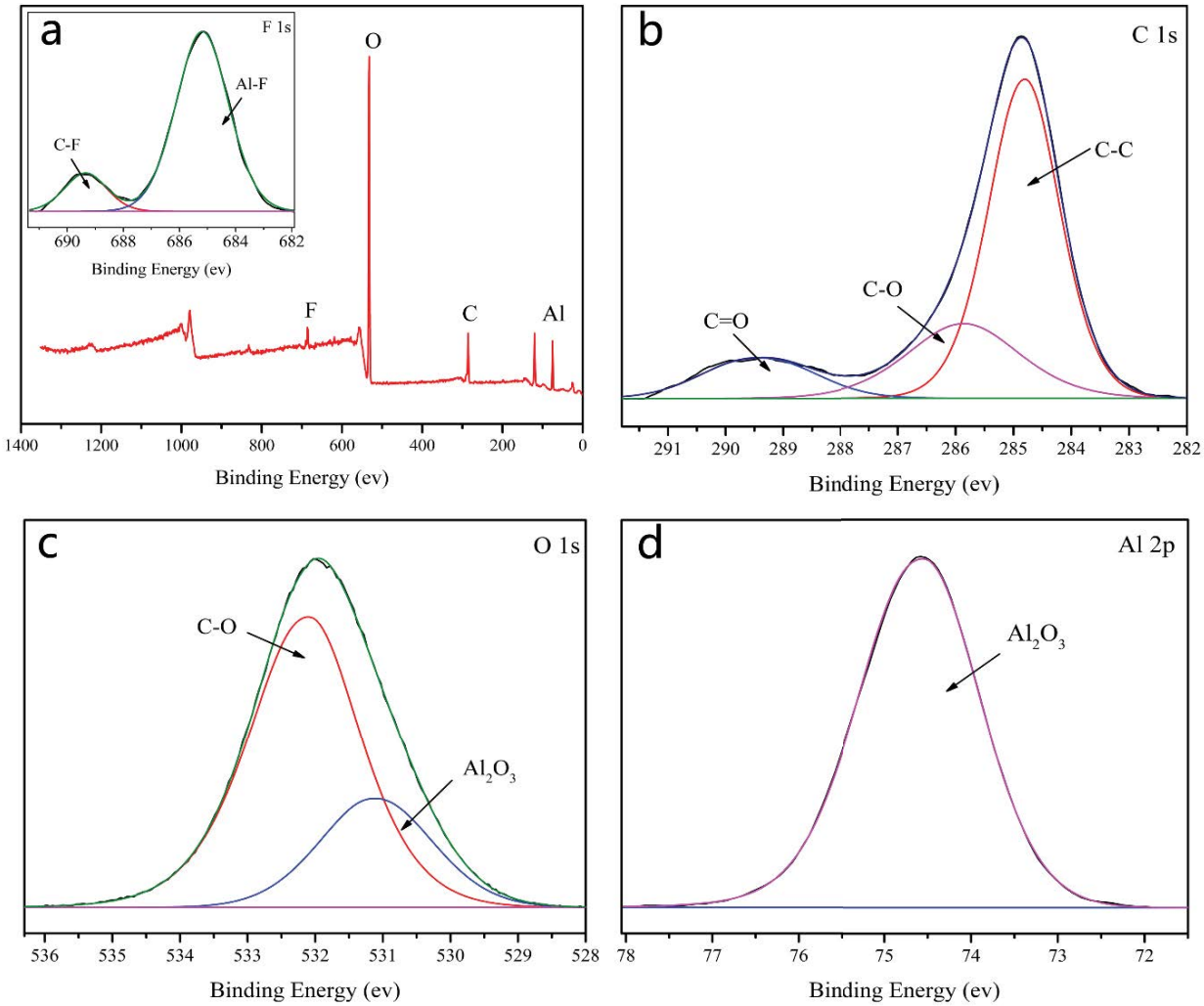

Fig. 10. XPS spectra of the AUG after adsorption: (a) full range spectrum and (inset) high-resolution of F 1s; high-resolution of (b) C 1s, (c) O 1s and (d) Al 2p.

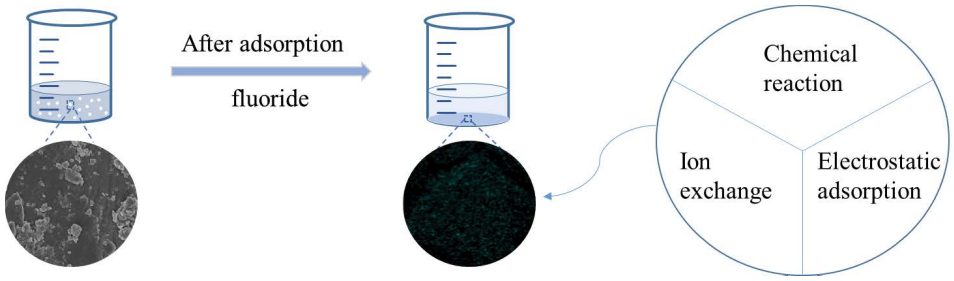

Fig. 11. Sketch of the AUG adsorption mechanism.

FTIR results shows that the absorption peak of the Al–O group at 927 cm^{-1} disappeared and the peak at 751 cm^{-1} decreased after adsorption, implying the involvement of Al (AlO_6) in the defluoridation process. It could also be observed that after adsorption the –OH changed from three peaks at 3,361; 3,132, and 3,042 cm^{-1} to one at 3,360 cm^{-1}, implying that this group played an important role in fluoride adsorption. After adsorption the intensity of the peaks for C=C and C=O also decreased significantly, suggesting that C=C and C=O may be involved in the fluoride adsorption process.

According to aforementioned characterization results and adsorption experiments, the mechanism of fluoride adsorption by AUG would be (Fig. 11): (1) Electrostatic attraction, a strong electrostatic attraction exists between

the negatively charged fluoride and the positively charged adsorbent surface in the pH range studied. (2) Ion-exchange reaction, there is an ion exchange between fluoride and C=C [47] as well as –OH. (3) Chemical reaction, the oxygen in the Al–O group (such as AlO_6) is replaced by fluorine ions to form $NaAlF_6$ with Al–F bonds.

4. Conclusions

In summary, herein AUG was applied as an defluoridation adsorbent with excellent performance based on a facile hydrothermal method. Its effective fluoride removal could be achieved at low doses and a wide pH range, from 5.0 to 8.0. The maximum capacity of AUG on fluoride adsorption could reach 107.7 mg/g, which is much higher than many reported adsorbents. The fluoride adsorption of AUG followed the Langmuir isotherm model, indicating its monolayer adsorption. We also demonstrated that the adsorption kinetics of AUG followed a pseudo-secondary kinetic model, dominated by chemisorption of fluoride. The additional mechanism of fluoride removal includes electrostatic attraction, ion exchange and chemical reaction with carbon-containing functional groups. Our study suggests that AUG could be a potential adsorbent for enhanced fluoride removal from drinking water.

Acknowledgment

This work was supported by National Natural Science Foundation of China (51078348) and Nantong Science and Technology Project (MS 12020076).

References

[1] L. Huang, Z. Luo, X. Huang, Y. Wang, J. Yan, W. Liu, Y. Guo, S.R. Babu Arulmani, M. Shao, H. Zhang, Applications of biomass-based materials to remove fluoride from wastewater: a review, Chemosphere, 301 (2022) 134679, doi: 10.1016/j.chemosphere.2022.134679.

[2] X. Tang, C. Zhou, W. Xia, Y. Liang, Y. Zeng, X. Zhao, W. Xiong, M. Cheng, Z. Wang, Recent advances in metal–organic framework-based materials for removal of fluoride in water: performance, mechanism, and potential practical application, Chem. Eng. J., 446 (2022) 137299, doi: 10.1016/j.cej.2022.137299.

[3] S.I. Alhassan, L. Huang, Y. He, L. Yan, B. Wu, H. Wang, Fluoride removal from water using alumina and aluminum-based composites: a comprehensive review of progress, Crit. Rev. Env. Sci. Technol., 51 (2021) 2051–2085.

[4] J. Danziger, L.E. Dodge, H. Hu, Role of renal function in the association of drinking water fluoride and plasma fluoride among adolescents in the United States: NHANES, 2013–2016, Environ. Res., 213 (2022) 113603, doi: 10.1016/j.envres.2022.113603.

[5] M. Abtahi, S. Dobaradaran, S. Jorfi, A. Koolivand, S.S. Khaloo, J. Spitz, H. Saeedi, N. Golchinpour, R. Saeedi, Age-sex specific disability-adjusted life years (DALYs) attributable to elevated levels of fluoride in drinking water: a national and subnational study in Iran, 2017, Water Res., 157 (2019) 94–105.

[6] K. Wan, L. Huang, J. Yan, B. Ma, X. Huang, Z. Luo, H. Zhang, T. Xiao, Removal of fluoride from industrial wastewater by using different adsorbents: a review, Sci. Total Environ., 773 (2021) 145535, doi: 10.1016/j.scitotenv.2021.145535.

[7] Y. Zhao, Q. Song, T. Ma, Z. Tian, M. Ji, Research progress in the modified/novel fluoride adsorbing materials, Ind. Water Treat., 38 (2018) 9–14.

[8] D. Khandare, S. Mukherjee, A review of metal oxide nanomaterials for fluoride decontamination from water environment, Mater. Today Proc., 18 (2019) 1146–1155.

[9] J. He, F. Zhang, S. Han, X. Li, X. Yao, H. Zhang, The distribution and genetic types of high-fluoride groundwater in northern China, Geology, 37 (2010) 621–626.

[10] L.N. Affonso, J.L. Marques, V.V.C. Lima, J.O. Gonçalves, S.C. Barbosa, E.G. Primel, T.A.L. Burgo, G.L. Dotto, L.A.A. Pinto, T.R.S. Cadaval Jr., Removal of fluoride from fertilizer industry effluent using carbon nanotubes stabilized in chitosan sponge, J. Hazard. Mater., 388 (2020) 122042, doi: 10.1016/j.jhazmat.2020.122042.

[11] B. Zhao, Y. Zhang, X. Dou, X. Wu, M. Yang, Defluoridation performance and application of granular Fe-Al-Ce trimetal oxide adsorbent by extrusion method for fluoride removal from groundwater, Chin. J. Environ. Eng., 7 (2013) 2801–2807.

[12] K. Xu, J. Lu, I.D. Tegladza, Q. Xu, Z. Yang, G. Lv, Combined metal/air fuel cell and electrocoagulation process: energy generation, flocs production and pollutant removal, Chemosphere, 255 (2020) 126925, doi: 10.1016/j.chemosphere.2020.126925.

[13] J. Nunes-Pereira, R. Lima, G. Choudhary, P.R. Sharma, S. Ferdov, G. Botelho, R.K. Sharma, S. Lanceros-Méndez, Highly efficient removal of fluoride from aqueous media through polymer composite membranes, Sep. Purif. Technol., 205 (2018) 1–10.

[14] F. Zhu, Z. Guo, X. Hu, Fluoride removal efficiencies and mechanism of schwertmannite from $KMnO_4$/MnO_2–Fe(II) processes, J. Hazard. Mater., 397 (2020) 122789, doi: 10.1016/j.jhazmat.2020.122789.

[15] N.A. Medellin-Castillo, R. Leyva-Ramos, E. Padilla-Ortega, R.O. Perez, J.V. Flores-Cano, M.S. Berber-Mendoza, Adsorption capacity of bone char for removing fluoride from water solution. Role of hydroxyapatite content, adsorption mechanism and competing anions, J. Ind. Eng. Chem., 20 (2014) 4014–4021.

[16] P. Dhanasekaran, O. Sahu, Arsenate and fluoride removal from groundwater by sawdust impregnated ferric hydroxide and activated alumina (SFAA), Groundwater Sustainable Dev., 12 (2020) 100490, doi: 10.1016/j.gsd.2020.100490.

[17] S.M. Maliyekkal, A.K. Sharma, L. Philip, Manganese-oxide-coated alumina: a promising sorbent for defluoridation of water, Water Res., 40 (2006) 3497–3506.

[18] S.S. Tripathy, J.L. Bersillon, K. Gopal, Removal of fluoride from drinking water by adsorption onto alum-impregnated activated alumina, Sep. Purif. Technol., 50 (2006) 310–317.

[19] J. He, Y. Xu, Z. Xiong, B. Lai, L. Yang, The enhanced removal of phosphate by structural defects and competitive fluoride adsorption on cerium-based adsorbent, Chemosphere, 256 (2020) 127056, doi: 10.1016/j.chemosphere.2020.127056.

[20] U.S. Rashid, A.N. Bezbaruah, Citric acid modified granular activated carbon for enhanced defluoridation, Chemosphere, 252 (2020) 126639, doi: 10.1016/j.chemosphere.2020.126639.

[21] C. Ding, F. Xu, F. Liu, H. Wang, Y. Jiang, B. Sun, S. Zhu, The preparation of iron-aluminum double hydroxide and study on fluoride removal in water, Environ. Dev., 31 (2019) 90–93,95.

[22] H. Jiang, X. Li, L. Tian, T. Wang, Q. Wang, P. Niu, P. Chen, X. Luo, Defluoridation investigation of Yttrium by laminated Y-Zr-Al tri-metal nanocomposite and analysis of the fluoride sorption mechanism, Sci. Total Environ., 648 (2019) 1342–1353.

[23] M. Kim, C.E. Choong, S. Hyun, C.M. Park, G. Lee, Mechanism of simultaneous removal of aluminum and fluoride from aqueous solution by La/Mg/Si-activated carbon, Chemosphere, 253 (2020) 126580, doi: 10.1016/j.chemosphere.2020.126580.

[24] R.S. Sathish, N.S.R. Raju, G.S. Raju, G. Nageswara Rao, K.A. Kumar, C. Janardhana, Equilibrium and kinetic studies for fluoride adsorption from water on zirconium impregnated coconut shell carbon, Sep. Sci. Technol., 42 (2007) 769–788.

[25] W.X. Gong, J.H. Qu, R.P. Liu, H.C. Lan, Adsorption of fluoride onto different types of aluminas, Chem. Eng. J., 189–190 (2012) 126–133.

[26] D. Kang, X. Yu, M. Ge, M. Lin, X. Yang, Y. Jing, Insights into adsorption mechanism for fluoride on cactus-like amorphous alumina oxide microspheres, Chem. Eng. J., 345 (2018) 252–259.

[27] G.F. El-Said, E.-S.M. Abdelrehim, M.E.-S. Elba, S.M.H.A. Kawy, A critical study of interactive fluoride adsorption by raw marine organisms and a synthetic organic 2-amino-3-cyano-4(4-nitrophenyl)-6-phenylpyridine as adsorbent tools, Environ. Monit. Assess., 191 (2019) 311, doi: 10.1007/s10661-019-7465-5.
[28] C. Lei, X. Zhu, B. Zhu, C. Jiang, Y. Le, J. Yu, Superb adsorption capacity of hierarchical calcined Ni/Mg/Al layered double hydroxides for Congo red and Cr(VI) ions, J. Hazard. Mater., 321 (2017) 801–811.
[29] X. Yu, D. Kang, Y. Hu, S. Tong, M. Ge, C. Cao, W. Song, One-pot synthesis of porous magnetic cellulose beads for the removal of metal ions, RSC Adv., 4 (2014) 31362–31369.
[30] M. Casamassima, E. Darque-Ceretti, A. Etcheberry, M. Aucouturier, Acid—base behavior of aluminum and silicon oxides — a combination of two approaches: XPS and Lewis acido-basicity; rest potential and Brönsted acido-basicity, Appl. Surf. Sci., 52 (1991) 205–213.
[31] Y. Sun, S. Yang, C. Ding, Z. Jin, W. Cheng, Tuning the chemistry of graphene oxides by a sonochemical approach: application of adsorption properties, RSC Adv., 5 (2015) 24886–24892.
[32] P.K. Sharma, M. Jilavi, D. Burgard, R. Nass, H. Schmidt, Hydrothermal synthesis of nanosize α-Al_2O_3 from seeded aluminum hydroxide, J. Am. Ceram. Soc., 81 (1998) 2732–2734.
[33] Y.-X. Zhang, Y. Jia, Preparation of porous alumina hollow spheres as an adsorbent for fluoride removal from water with low aluminum residual, Ceram. Int., 42 (2016) 17472–17481.
[34] Y. Sun, D. Shao, C. Chen, S. Yang, X. Wang, Highly efficient enrichment of radionuclides on graphene oxide-supported polyaniline, Environ. Sci. Technol., 47 (2013) 9904–9910.
[35] M. Zhang, Q. Yao, C. Lu, Z. Li, W. Wang, Layered double hydroxide-carbon dot composite: high-performance adsorbent for removal of anionic organic dye, ACS Appl. Mater. Interfaces, 6 (2014) 20225–20233.
[36] U. Kumari, S.K. Behera, B.C. Meikap, A novel acid modified alumina adsorbent with enhanced defluoridation property: kinetics, isotherm study and applicability on industrial wastewater, J. Hazard. Mater., 365 (2019) 868–882.
[37] H.M. Cai, G.J. Chen, C.Y. Peng, Z.Z. Zhang, Y.Y. Dong, G.Z. Shang, X.H. Zhu, H.J. Gao, X.C. Wan, Removal of fluoride from drinking water using tea waste loaded with Al/Fe oxides: a novel, safe and efficient biosorbent, Appl. Surf. Sci., 328 (2015) 34–44.
[38] F. Li, J. Jin, Z. Shen, H. Ji, M. Yang, Y. Yin, Removal and recovery of phosphate and fluoride from water with reusable mesoporous Fe_3O_4@mSiO_2@mLDH composites as sorbents, J. Hazard. Mater., 388 (2020) 121734, doi: 10.1016/j.jhazmat.2019.121734.
[39] Z. Jian, W. Zhu, Y. Jie, H. Zhang, Y. Zhang, X. Lin, X. Luo, Highly selective and efficient removal of fluoride from ground water by layered Al-Zr-La tri-metal hydroxide, Appl. Surf. Sci., 435 (2017) 920–927.
[40] L. Chai, Y. Wang, Z. Na, W. Yang, X. You, Sulfate-doped Fe_3O_4/Al_2O_3 nanoparticles as a novel adsorbent for fluoride removal from drinking water, Water Res., 47 (2013) 4040–4049.
[41] S. Guiza, F. Brouers, M. Bagane, Fluoride removal from aqueous solution by montmorillonite clay: kinetics and equilibrium modeling using new generalized fractal equation, Environ. Technol. Innovation, 21 (2020) 101187, doi: 10.1016/j.eti.2020.101187.
[42] L. Yan, W. Gu, N. Zhou, C. Ye, Y. Yang, Preparation and characterization of wheat straw biochar loaded with aluminium/lanthanum hydroxides: a novel adsorbent for removing fluoride from drinking water, Environ. Technol., 43 (2022) 2771–2784.
[43] X. Dou, D. Mohan, C.U. Pittman, Jr., S. Yang, Remediating fluoride from water using hydrous zirconium oxide, Chem. Eng. J., 198 (2012) 236–245.
[44] G. Mekhemer, Characterization of phosphated zirconia by XRD, Raman and IR spectroscopy, Colloids Surf., A, 141 (1998) 227–235.
[45] L. Liu, X. Qi, S. Yin, Q. Zhang, Y.S. Hu, *In-situ* formation of stable interface in solid-state batteries, ACS Energy Lett., 4 (2019) 1650–1657.
[46] Y. Zhao, Y. Liu, Y. Chen, X. Liu, X. Li, S. Gao, A treasure map for nonmetallic catalysts: optimal nitrogen and fluorine distribution of biomass-derived carbon materials for high-performance oxygen reduction catalysts, J. Mater. Chem. A, 9 (2021) 18251–18259.
[47] M. Ye, Y. Cao, R. Ding, Z. Lei, L. Jin, J. Zhang, Soft hard acid–base theory and its application, Chem. Ind. Times, 33 (2019) 28–31.